Chinese Chemical Letters 31 (2020) 3200–3204

Contents lists available at ScienceDirect

Chinese Chemical Letters

journal homepage: www.elsevier.com/locate/cclet

Communication

Excess capacity on compound phases of Li_2FeTiO_4 composite cathode materials synthesized by hydrothermal reaction using optional titanium sources to boost battery performance

Liu Yang[a,b,c], Shaohua Luo[b,c,d,*], Yafeng Wang[a,b,c], Yang Zhan[a,b,c], Qing Wang[b,c,d,*], Yahui Zhang[b,c,d], Xin Liu[a,b,c,d], Wenning Mu[b,d], Fei Teng[b,d]

[a] School of Materials Science and Engineering, Northeastern University, Shenyang 110819, China
[b] School of Resources and Materials, Northeastern University at Qinhuangdao, Qinhuangdao 066004, China
[c] Key Laboratory of Dielectric and Electrolyte Functional Material Hebei Province, Qinhuangdao 066004, China
[d] Qinhuangdao Laboratory of Resources Cleaner Conversion and Efficient Utilization, Qinhuangdao 066004, China

ARTICLE INFO

Article history:
Received 12 March 2020
Received in revised form 16 May 2020
Accepted 24 May 2020
Available online 26 May 2020

Keywords:
Li_2FeTiO_4 nanocomposites
Cathode materials
Hydrothermal reaction
Lithium ion battery
Post-heat-treatment

ABSTRACT

Li_2FeTiO_4 composites have been produced using commercial LiAC, $FeCl_2$ and different titanium sources by hydrothermal synthesis (HS) at 175 °C and subsequent annealing at 700 °C. Impure phase TiO_2, Fe_2O_3 and $FeTiO_4$ were detected out among the Li_2FeTiO_4 composites with different titanium sources. Micron and nano-sized particles of Li_2FeTiO_4 were prepared from various titanium raw materials, with nano-sized particles predominating when titanium raw materials were layered hydrogen titanate nanowire ($H_2Ti_3O_7$NW, HTO-NW) and titanium oxide nanotubes (TiO_2NB). The Li_2FeTiO_4 composites synthesized by HTO-NW shows a primary particle size of 50–200 nm of high crystallinity staggered with undissolved nanowire with a diameter size of about 100 nm. The samples using one-dimensional nanometer titanium oxide (TiO_2 NB) as the raw material can get a super high initial discharge capacity of 367.8 mAh/g at the rate of C/10 and excellent cycling stability. The selection of raw materials and adopting multi-phase modification can be considered as an effective strategy to improve the electro-chemical properties of Li_2FeTiO_4 composite cathode materials for the lithium secondary battery.

Currently, titanate-based compounds have been considered as hopeful materials for high-performance lithium-ion batteries, then the new category of lithium-rich transition metal oxides Li_2MTiO_4 (M = Fe, Mn, Co, Ni or Cu) have excellent theoretical capacity (about 290 mAh/g), and have been researched as cathode materials for lithium batteries [1–7]. Among these oxides, the redox reaction of $Ti^{4+} + M^{2+} \leftrightarrow Ti^{3+} + M^{3+}$ is beneficial to the high capacity of Ti^{4+}/M^{2+} oxidation states in principle, and it realized the two-electron response of each Fe atom [8,9]. Among these cubic cations disordered rock salt (space group Fm-3m) structure materials, the metal atoms in Li_2FeTiO_4 are disordered in octahedral sites of the cubic closet packing (CCP) array of anions [10]. Li_2FeTiO_4 cathode materials had been attracted attention for the environment friendly, low-cost and high theoretical capacity [11]. However, it is difficult for the Li_2FeTiO_4 to attain its full capacity, because of low electron conductivity and slow diffusion rate of Li^+ in the olivine structure. To solve these problems, people have made a lot of efforts, one of the most effective methods is fabricating nanostructure [12–15]. Lithium-ionbattery electrodes prepared by nanomaterials or mesoporous nanocomposites have excellent rate capability [16–23]. For example, Yang *et al.* [24] use nanostructured Li_2FeTiO_4/graphene composites made by sol-gel method with graphene oxide as the template and distributed on the graphene substrate, and the particle size was 20–50 nm. Kuzma *et al.* [25] reported that novel active materials were made by using transition metal titanates (Li_2MTiO_4) as carbon precursor, which consist of 10–20 nm particles embedded in the conductive carbon coating. They also show that it is not the coating but the size of the small particles determines the activity of electrode materials. However, using graphene oxide or carbon precursor to obtain products usually requires multi-steps and special treatment, which was not commercially viable.

The morphology and size of nanomaterials play an important role in the electrochemical properties [26–28]. The electrode material made by the hydrothermal method with uniform particle

* Corresponding authors.
E-mail addresses: tianyanglsh@163.com (S. Luo), wangswork@126.com (Q. Wang).

https://doi.org/10.1016/j.cclet.2020.05.036
1001-8417/

size distribution, stable electro-chemical properties, and structure can be controlled, which is easy to realize the nano-crystallization of electrode materials and expected to achieve the industrial production of materials [29–38]. In this paper, Li_2FeTiO_4 composite materials adopting multi-phase modification synthesized by hydrothermal, and the reinforcing agent formed by the growth of the multi-phase modification constitutes the multi-phase composite materials with a super high initial discharge capacity and excellent cycling stability [39]. Li_2FeTiO_4 composite cathode materials have high crystallinity, high specific surface area and uniform particle size, which make it had much superior electrochemical performances than most of the reported $Li_4Ti_5O_{12}$-based nanocomposites. Well-dispersed Li_2FeTiO_4 composite particles were successfully prepared by the hydrothermal reaction method using tetrabutyl titanate, TiO_2 anatase, hydrogen titanate nanowire ($H_2Ti_3O_7$NW, HTO-NW) and titanium oxide nanotubes (TiO_2 NB) as the source of titanium. Because different raw materials have a significant influence on the electro-chemical characterization of Li-ion batteries [40], we use different titanium source preparations of Li_2FeTiO_4 in a performance comparison to determine the best reaction materials. The products of Li_2FeTiO_4 have high yield and good industrial application prospects.

The schematic diagram of the preparation procedure of Li_2FeTiO_4 composite cathode materials is presented at Fig. S1 (Supporting information). Commercial LiAC, $FeCl_2$, tetrabutyl titanate or TiO_2 anatase, hydrogen titanate nanowire ($H_2Ti_3O_7$NW, HTO-NW) and titanium oxide nanotubes (TiO_2 NB) were mixed in designed molar ratio as 4:1:1 for the hydrothermal method. The mixtures were filled in a Teflon vessel (110 mL). The vessel was placed in a stainless-steel autoclave and heated with 180−220 °C. After cooling to room temperature, the precipitates were collected by suction filtration and dried in vacuum. In the post-heat-treatment, dried products were calcined under nitrogen atmosphere at 700 °C for 10 h. The electrolyte was 1 mol/L $LIPF_6$ synthesized by ethylene carbonate, dimethyl carbonate and ethyl methyl carbonate with volume ratio of 1:1:1, the water content of electrolyte was 10 ppm. The battery was the button battery of CR2025. In addition, commercial LiAC was supplied by the Third Tianjin Chemical Reagent Factory with AR grade purity; $FeCl_2$ was supplied by Tianjin Damao Chemical Reagent Factory with AR grade purity; tetrabutyl titanate was supplied by Tianjin Guangfu Fine Chemical Research Institute with AR grade purity and TiO_2 anatase was supplied by Beijing Modern Oriental Company with AR grade purity. Hydrogen titanate nanowire ($H_2Ti_3O_7$NW, HTO-NW) was prepared by mixing solution of TiO_2 anatase and NaOH (NaOH was supplied by Beijing Modern Oriental Company with AR grade purity) in ultrasonic generator for 2 h (ultrasonic power is 0.2–0.5 W/cm^2) and then placed at 150 ℃ for 48 h. Titanium oxide nanotubes (TiO_2 NB) was prepared from hydrogen titanate nanowire after heat treatment at 700 °C.

The crystal structure of Li_2FeTiO_4 composites were determined bypowder X-ray diffraction (XRD) using Cu-Kα radiation (λ = 0.15406 nm) at scan rate of 0.04°/s (30 kV) with DX-2500 instrument. The morphology of samples were observed and compared using field-emission scanning electron microscopy (FE-SEM, S-4800-II, Hitachi, Japan). The Li_2FeTiO_4 was mixed with acetylene black and polyvinylidene difluoride (PVDF) at the weight ratio of 75:17:8 to prepare electrodes in *N*-methyl pyrrolidone. The loading mass of active material is 1.96 mg. A LAND CT 2001A system was utilized for battery charge-discharge tests between 1.5 V and 4.8 V *vs.* Li, and the battery was cycled galvanostatically at room temperature. The specific surface area was determined and the particle size was analyzed under 175 °C constant temperature of liquid nitrogen using SSA-4300 instrument. The specific surface area of the Li_2FeTiO_4 was calculated from N_2 adsorption/desorption data by Brunauer-Emmett-Teller (BET) method and the pore size distribution can be obtained by Barrett-Joyner-Halenda (BJH) method. Electro-chemical impedance spectroscopy (EIS) and cyclic voltammetry (CV) were obtained by Solartron 1260 + 1287 electro-chemical impedance analyzer.

Fig. 1 shows the XRD pattern of Li_2FeTiO_4 composite cathode materials under hydrothermal conditions. The main reflectance peaks are attributed to the Li_2FeTiO_4 phase, that means the samples have irregular rock-salt-type structure. Three intense diffraction peaks corresponding to the (111), (200) and (222) planes are consistent with reported data [25], demonstrate that synthetic materials are made of Li_2FeTiO_4. Impure phase TiO_2, Fe_2O_3 and $FeTiO_4$ were detected among the Li_2FeTiO_4 composites with different titanium sources. The observation of such impurities has also been reported by other authors, and it is a common problem with the hydrothermal reaction method [24,25]. These impurities are used for multi-phase modification of Li_2FeTiO_4 composite materials, and particle dispersion of multi-phase materials make up for uneven distribution caused by differences in the morphology of the nanotubes. The unmarked small peaks in Fig. 1 are the impurity peaks, which have little influence on the material properties. Besides, Li_2FeTiO_4 materials with complete phase structure cannot be synthesized from tetrabutyl titanate, and this sample will not be discussed.

Figs. 2a–c show the morphological features of Li_2FeTiO_4 composite cathode materials (SEM), and Figs. 2d–f are the corresponding pore size distribution profile, which shows the grain size. When the grain size is smaller, the specific surface area of the Li_2FeTiO_4 is more significant, which can efficiently increase the active sites of charge-discharge reaction between Li_2FeTiO_4 and electrolyte. The products synthesized by TiO_2 anatase have the largest grain size, followed by HTO-NW and TiO_2 NB. The synthesis grain size of HTO-NW and TiO_2 NB is relatively small, but the grain distribution of HTO-NW is not uniform, the condensation phenomenon is serious, and products still retain titanate nanowire morphology. The larger grain size, the more easily affect electro-chemical properties of the electrode materials [11]. The materials synthesized from TiO_2 NB have homogeneous and loose particles growth density. It indicates that materials of TiO_2 NB can obtain the target material of small particles.

The specific surface area determined by the BET method is shown in Figs. 2g–i. The results show that specific surface area of Li_2FeTiO_4 samples prepared by TiO_2 anatase, HTO-NW and TiO_2 NB are 7.699 m^2/g, 16.054 m^2/g and 12.938 m^2/g, respectively. The surface area curves of three Li_2FeTiO_4 samples made by different materials are similar. The nitrogen adsorption-desorption

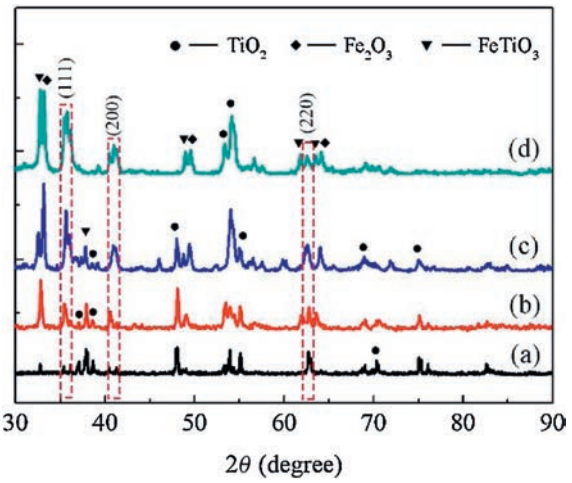

Fig. 1. XRD of Li_2FeTiO_4composite cathode materials synthesized from (a) tetrabutyl titanate, (b) TiO_2 anatase, (c) HTO-NW and (d) TiO_2 NB.

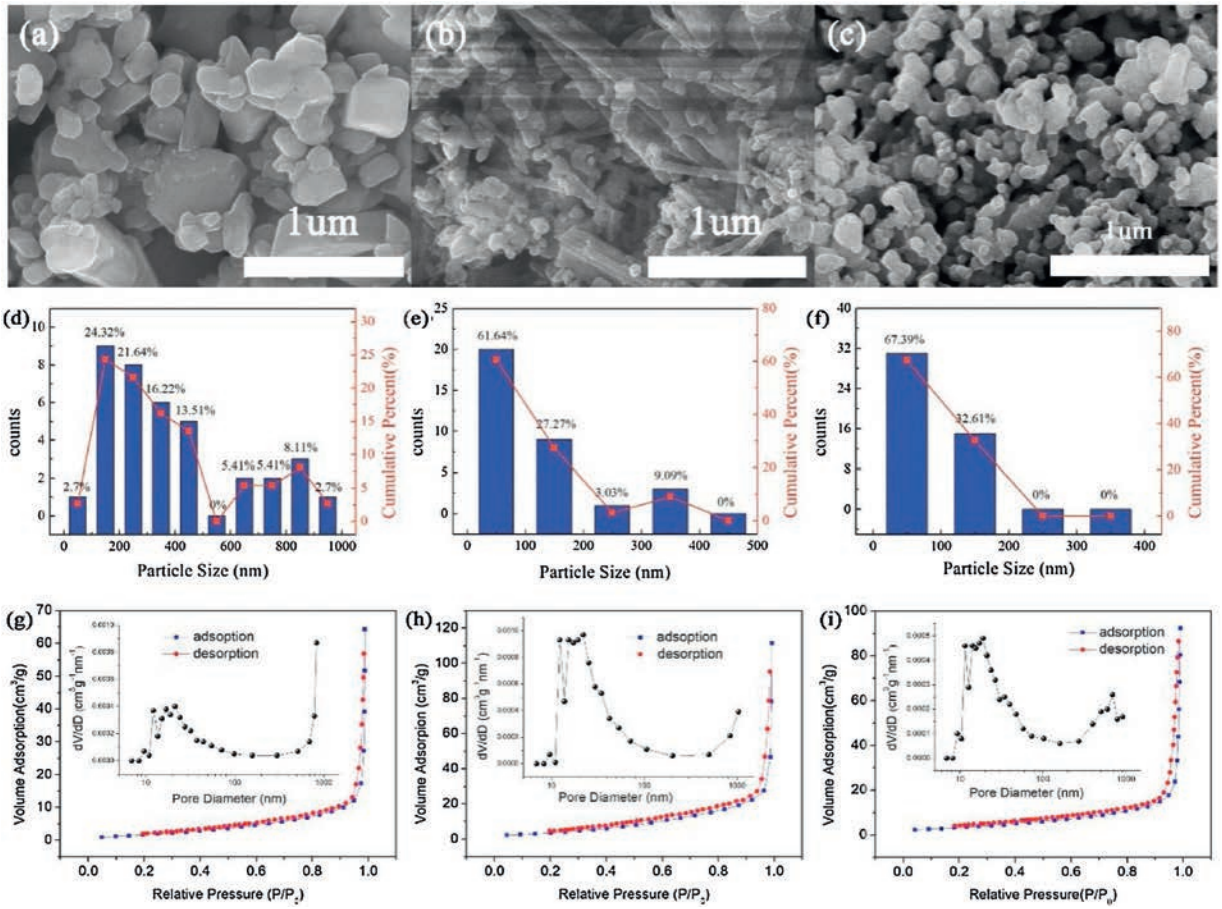

Fig. 2. SEM particle size distribution and nitrogen adsorption/desorption isotherms (inset: pore size distribution profile) of Li_2FeTiO_4 synthesized from (a, d, g) TiO_2 anatase, (b, e, h) HTO-NW and (c, f, i) TiO_2 NB.

isotherms of all Li_2FeTiO_4 samples can be categorized as typical type IV isotherm, and the H3 hysteres is loop exists under relative pressure of 0-1, indicates that existence of mesoporous structure. The adsorption amount is very low at the low-pressure area, meaning that the interaction between adsorbent and adsorbate is weak. With the increase of pressure, the adsorption amount increased sharply, which indicates that the pores are filled. The large surface area of Li_2FeTiO_4 samples prepared by HTO-NW and TiO_2 NB provide more active sites for Li^+ insertion/extraction, and promotes effective contact area between electrode and electrolyte, improves reaction kinetics. Inset of Figs. 2g–i show the corresponding BJH pore size distribution plots of Li_2FeTiO_4 and they are consistent with the SEM images. The pore size profile of Li_2FeTiO_4 synthesized from HTO-NW and TiO_2 NB are uniform, and the number of grains with small grain size is much larger than the products synthesized from TiO_2 anatase. A large surface area can provide good liquid absorption capacity, which can effectively increase the area of electro-chemical reaction.

Fig. 3 shows the C/10 rate against lithium for three samples, and the dotted red line is the theoretical capacity (295 mAh/g) of Li_2FeTiO_4. The discharge cutoff potential is 4.5 and 1.0 V, and the charge-discharge current is 10 mA/g. The efficiency experiment shows that the first discharge capacity of Li_2FeTiO_4 prepared byTiO_2 NB and HTO-NWis 367.8 mAh/g and 246.7 mAh/g, are higher than it made by TiO_2 anatase (86.9 mAh/g). The samples using one-dimensional TiO_2 NB as the raw material can get a high initial discharge capacity compared with theoretical capacity. The initial Coulombic efficiency of TiO_2 NB as the raw material was 82.57%. For comparison, the electrochemical performance of

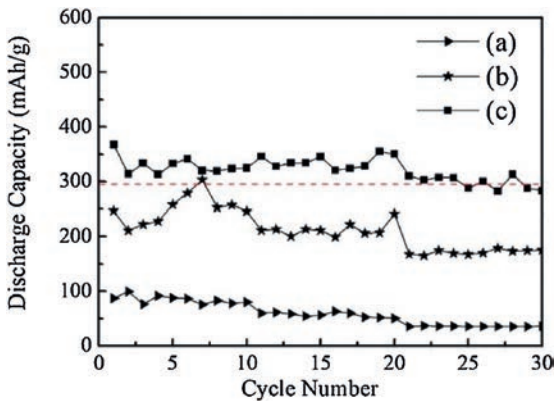

Fig. 3. Discharge capacity cycling performance of Li_2FeTiO_4 samples electrodes at C/10 rate. Li_2FeTiO_4 samples electrodes synthesized from (a) TiO_2 anatase, (b) HTO-NW and (c) TiO_2 NB.

Li_2FeTiO_4 prepared by TiO_2 NB in our work and the similar materials have been reported in the literature are summarized in Fig. S2 (Supporting information). The Li_2FeTiO_4 electrode in this work achieves an excellent specific capacity [41]. It can be seen from the Fig. 3, the structural stability of all electrode samples have slight change and the sample capacity have a certain attenuation. It is because that, Li^+ is regularly embedded and extracted at the process of charge-discharge, resulting in expansion and contraction accompanied by stress variations. In addition, as shown in

Figs. S3 and S4 (Supporting information), the Li_2FeTiO_4 cathode materials from raw materials of TiO_2 NB have good stability and rate properties.

The representative discharge/charge curves of Li_2FeTiO_4 samples for the 1st, 2nd, 5th, 10th and 20th cycles at a current density of 0.1 A/g are shown in Fig. 4. The initial discharge capacities of Li_2FeTiO_4 samples prepared by TiO_2 anatase, HTO-NW and TiO_2 NB are 99.2, 211.0 and 313.5 mAh/g, respectively. The properties of samples prepared from HTO-NW and TiO_2 NB materials are far better than TiO_2 anatase. The reason for the different shapes of charge and discharge curves of the three materials is that the grain sizes of different titanium sources materials are different, which affects the electro-chemical property of Li_2FeTiO_4 samples. In first discharge process, the Li_2FeTiO_4 samples prepared by TiO_2 NB electrode have a good reversible discharge capacity of 313.5 mAh/g, higher than single electron Fe^{3+}/Fe^{2+} reaction [31]. The Li_2FeTiO_4 samples show a size-dependent excess capacity (beyond the theoretical value of 295 mAh/g) in samples synthesized from TiO_2 NB with mean particle sizes of 67.6 nm. The discharge capacity of Li_2FeTiO_4 samples prepared by TiO_2 NB in the second cycle is about 333.2 mAh/g, and the discharge capacity decreases to 324.4 mAh/g after 10 cycles, it demonstrates that the stability of Li_2FeTiO_4 samples. It is worth noting that, after 20 cycles, the capacity returns to 341 mAh/g, which may be due to a pseudo reaction on the surface of the active substance. The high discharge capacity and stability of the Li_2FeTiO_4 samples prepared by TiO_2 NB suggest that Li_2FeTiO_4 composite materials can be used as the excellent cathode material.

Fig. 4d shows the cyclic voltammogram (CV) curves of Li_2FeTiO_4 synthesized from TiO_2 NB (scanning rate is 0.1 mV/s), which have a visible redox peak. During the Li^+ insertion/extraction process, a distinct cathode peak appeared at 1.68 V in the initial cycle, which was caused by the formation of Li_2FeTiO_4 and the transition from Fe^{3+} to Fe^{2+}. Furthermore, anode peak was found at 2.06 V during the process of gradual oxidation. The curves of the second and third cycles coincide well, indicates that the electro-chemical reaction of Li_2FeTiO_4 has good reversibility, which results that Li_2FeTiO_4 electrode has good stability.

The important electro-chemical performance parameters of Li_2FeTiO_4 composite electrode materials can be obtained by electro-chemical impedance spectroscopy (EIS). The Nyquist plots were shown in Fig. S5 (Supporting information). The operating conditions were the ac voltage amplitude of ± 10 mV and the frequency of 10^{-1}~10^5 Hz. There was no significant difference in EIS spectrum of Li_2FeTiO_4 composite materials prepared from different materials. According to calculation, the lithium ion diffusion coefficient of Li_2FeTiO_4 composite cathode materials prepared by TiO_2 NB is 1.62×10^{-12} cm^2/s. In Fig. S5, the figure is a straight line in the low-frequency range and semicircle shape in the high-frequency range. The impedance at high frequency corresponds to the resistance of electrolyte (R_1), and the intercept at semicircle corresponds to the charge transfer resistance (R_2). The double-layer capacitance (CPE) is a constant phase element, which indicates the charge accumulation on both sides of electrode and electrolyte interface [42]. Because the concave semicircle can be observed in Fig. S5, the CPE can be used to replace the pure capacitance. Besides, the sloped line in the low-frequency region was related to the diffusion of Li^+ in the electrode, and it can be attributed to the Warburg impedance (W_1). Inset picture of Fig. S5 represents the best fitting equivalent circuit, which can be expressed as follows:

$$R_1 + (R_2||CPE_1) + W_1$$

The R_2 of Li_2FeTiO_4 electrodes synthesized from titanium sources of TiO_2 NB is markedly lower than Li_2FeTiO_4 electrodes manufactured from HTO-NW and TiO_2 anatase, indicating that Li_2FeTiO_4 electrodes synthesized of TiO_2 NB have high electrical conductivity and fast charge transfer process. As shown in Figs. S5 and S6 (Supporting information), there were small differences between the different samples before and after the cycle. This

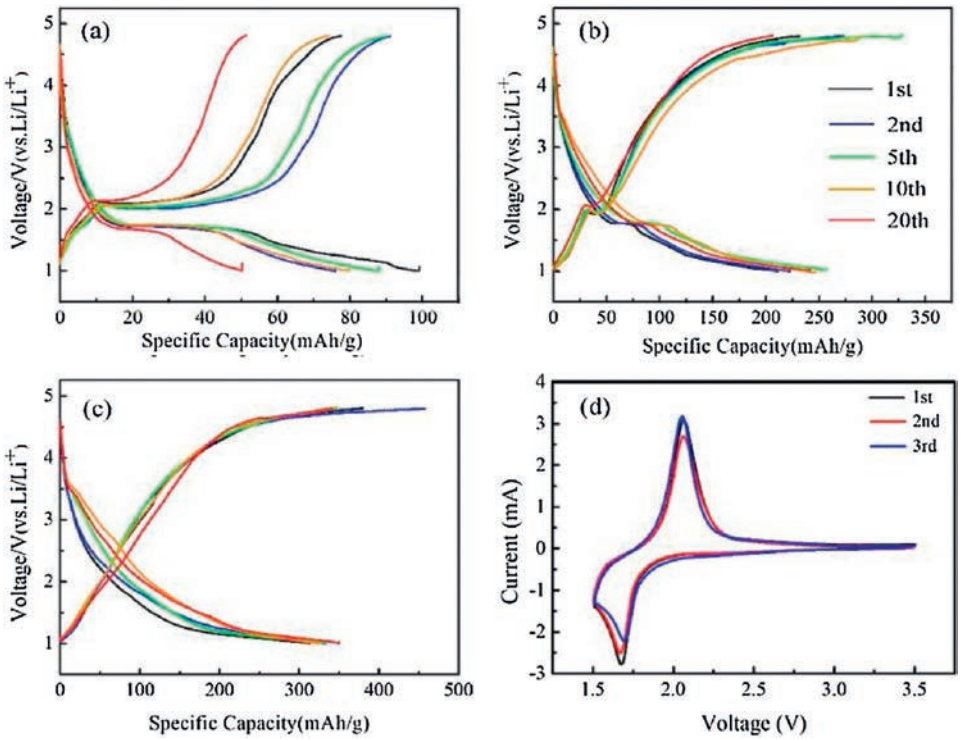

Fig. 4. Charge/discharge curves of Li_2FeTiO_4 samples electrodes synthesized from (a) TiO_2 anatase, (b) HTO-NW and (c) TiO_2 NB. (d) Cyclic voltammetry profiles of sample electrodes from TiO_2 NB.

demonstrates that Li_2FeTiO_4 electrodes synthesized of TiO_2NB have high electrical conductivity and fast charge transfer process.

The experimental design proposed herein enables the assessment of Li_2FeTiO_4 from raw materials of HTO-NW and TiO_2 NB, which have good electro-chemical performances compared with TiO_2 anatase. The Li_2FeTiO_4 composites material shows a primary particle size of 50−200 nm of high crystallinity staggered. The specific surface area of Li_2FeTiO_4 was measured *via* nitrogen adsorption/desorption isotherms, demonstrating the potential application of Li_2FeTiO_4 and the synthesis grain size of HTO-NW and TiO_2 NB were relatively small and uniform. As shown in Fig. S7 (Supporting information), the specific capacity of optimized Li_2FeTiO_4 cathode materials from raw materials of TiO_2 NB reached 367.8 mAh/g, and it showed good circular performance in the discharge process at C/10 rate. Therefore, Li_2FeTiO_4 cathode materials synthesized from HTO-NW and TiO_2 NB had good properties.

Declaration of competing interest

No conflict of interest exits in the submission of this manuscript, and manuscript is approved by all authors for publication. I would like to declare on behalf of my co-authors that the work described was original research that has not been published previously, and not under consideration for publication elsewhere, in whole or in part.

Acknowledgments

This work was financially supported by the National Natural Science Foundation of China (Nos. 51874079, 51674068), Natural Science Foundation of Hebei Province (No. E2018501091), The Training Foundation for Scientific Research of Talents Project, Hebei Province (No. A2016005004), The Fundamental Research Funds for the Central Universities (Nos. N172302001, N182312007, N182306001), Hebei Province Key Research and Development Plan Project (No. 19211302D), Qinhuangdao City University Student of Science and Technology Innovation and Entrepreneurship Project (Nos. PZB1810008T-46, PZB1810008T-14).

Appendix A. Supplementary data

Supplementary material related to this article can be found, in the online version, at doi:https://doi.org/10.1016/j.cclet.2020.05.036.

References

[1] Y.S. Li, X. Cheng, Y. Zhang, J. Electrochem. Soc. 159 (2012) A69–A74.
[2] A. Shintaro, T. Taisuke, U. Koki, M. Isamu, J. Chem. Commun. 49 (2013) 2939–2941.
[3] J.Z. Li, S.H. Luo, Q. Wang, et al., Electrochim. Acta 289 (2018) 415–421.
[4] S. Litty, J. Gopalakrishnan, J. Solid State Chem. 172 (2003) 171–177.
[5] T.F. Yi, T.T. Wei, Y. Li, Y.B. He, Z.B. Wang, Energy Storage Mater. 26 (2020) 165–197.
[6] D.C. An, L. Shen, D.N. Lei, et al., J. Energy Chem. 31 (2019) 19–26.
[7] F.F. Huang, J.M. Ma, H.Y. Xia, et al., ACS Appl. Mater. Interfaces 11 (2019) 37357–37364.
[8] S. Bao, S.H. Luo, Z.Y. Wang, et al., Ceram. Int. 44 (2018) 22512–22519.
[9] R. Dominko, M. Bele, M. Gaberscek, et al., Electrochem. Commun. 8 (2006) 217–222.
[10] R. Dominko, C.V.A. Garrido, M. Bele, et al., J. Power Sources 196 (2011) 6856–6862.
[11] M. Kuezma, R. Dominko, D. Hanzel, et al., J. Electrochem. Soc. 156 (2009) A809–A816.
[12] H.B. Huang, S.H. Luo, C.L. Liu, et al., ACS Appl. Mater. Interfaces 10 (2018) 21281–21290.
[13] J. Zhang, S.H. Luo, L.L. Sui, et al., J. Alloys Compd. 768 (2018) 991–994.
[14] W. Wei, F.F. Jia, K.F. Wang, et al., Chin. Chem. Lett. 28 (2017) 324–328.
[15] L. Deng, W.H. Yang, S.X. Zhou, et al., Chin. Chem. Lett. 26 (2015) 1529–1534.
[16] J. Li, Z. Tang, Z. Zhang, ChemInform 17 (2005) 5848–5855.
[17] J.Z. Li, S.H. Luo, Y. Sun, et al., Ceram. Int. 45 (2018) 4849–4856.
[18] S.C. Zhang, Y.L. Xing, T. Jiang, et al., J. Power Sources 196 (2011) 6915–6919.
[19] R.X. Lin, S.C. Zhang, Z.J. Du, et al., RSC Adv. 5 (2015) 87090–87097.
[20] S.C. Zhang, Z.J. Du, R.X. Lin, et al., Adv. Mater. 22 (2010) 5378–5382.
[21] X.M. Wu, S.C. Zhang, T. Qi, et al., J. Power Sources 307 (2016) 753–761.
[22] M.M. Sun, S.C. Zhang, T. Jiang, et al., Electrochem. Commun. 10 (2008) 1819–1822.
[23] H.B. Huang, S.H. Luo, C.L. Liu, et al., Electrochim. Acta 307 (2019) 232–240.
[24] M. Yang, X.Y. Zhao, C. Yao, et al., Mater. Technol. 31 (2016) 537–543.
[25] M. Kuezma, R. Dominko, A. Meden, et al., J. Power Sources 189 (2009) 81–88.
[26] J.Q. Liao, R. Tan, Z.X. Kuang, et al., Chin. Chem. Lett. 29 (2018) 1785–1790.
[27] H.Q. Dai, W.Q. Xu, K.H. Yu, W. Wei, Chin. Chem. Lett. 30 (2019) 517–520.
[28] Y.Y. Chen, B.J. Wang, T.Y. Hou, et al., Chin. Chem. Lett. 29 (2018) 187–190.
[29] K. Byrappa, T. Adschiri, Prog. Cryst. Growth Charact. Mater. 53 (2007) 117–166.
[30] M. Yoshimura, K. Byrappa, J. Mater. Sci. 43 (2008) 2085–2103.
[31] S.H. Luo, M. Wang, W.N. Sun, Ceram. Int. 38 (2012) 4325–4329.
[32] C.L. Liu, S.H. Luo, H.B. Wang, et al., J. Power Sources 389 (2018) 77–83.
[33] C.L. Liu, S.H. Luo, H.B. Wang, et al., ChemSusChem 4 (2019) 873–880.
[34] S.H. Luo, D.B. Hu, H. Liu, et al., J. Hazard. Mater. 368 (2019) 714–721.
[35] S.H. Luo, Y. Sun, S. Bao, et al., J. Electroanal. Chem. 832 (2019) 196–203.
[36] J.Z. Li, S.H. Luo, X. Ding, et al., Mater. Lett. 196 (2017) 183–186.
[37] X.G. Kong, J.R. Zhang, J.F. Huang, et al., Chin. Chem. Lett. 30 (2019) 771–774.
[38] R. Dang, X.L. Jia, P. Wang, et al., Chin. Chem. Lett. 28 (2017) 2263–2268.
[39] J.K. Guo, J. Mater. Res. 2 (2000) 123–126.
[40] D.M. Bao, H. Xiao, G.L. Zhou, New Chem. Mater. 36 (2008) 55–57.
[41] R.B. Shaun, C.K. Blakely, J.B. Clapham, et al., J. Power Sources 273 (2015) 396–403.
[42] M. Swietoslawski, M. Molenda, M. Grabowska, et al., Solid State Ionics 263 (2014) 99–102.